Improved three-way catalytic activity of bimetallic Ir-Rh catalyst supported on CeO2-ZrO2

Journal:	*Catalysis Science & Technology*
Manuscript ID:	CY-ART-11-2014-001502.R1
Article Type:	Paper
Date Submitted by the Author:	08-Dec-2014
Complete List of Authors:	Haneda, Masaaki; Nagoya Institute of Technology, Advanced Ceramics Research Center Kaneko, Takahiro; Nagoya Institute of Technologu, Kamiuchi, Naoto; Osaka University, Ozawa, Masakuni; Nagoya University,

Journal Name

RSCPublishing

ARTICLE

Improved three-way catalytic activity of bimetallic Ir-Rh catalyst supported on CeO_2-ZrO_2†

Cite this: DOI: 10.1039/xoxxoooooox

Masaaki Haneda,[a] Takahiro Kaneko,[a] Naoto Kamiuchi[b] and Masakuni Ozawa[c]

Received ooth January 2012,
Accepted ooth January 2012

DOI: 10.1039/xoxxoooooox

www.rsc.org/

The addition of a small amount of Ir caused a significant increase in not only CO and C_3H_6 oxidation activity but also NO reduction activity of Rh/CeO_2-ZrO_2 with the Ce/Zr molar ratio of 1/4 for NO-CO-C_3H_6-H_2-O_2 reaction in a stoichiometric condition. The optimum Ir/Rh atomic ratio was 1/9. Ir additive was found to suppress the preferential oxidation of CO and C_3H_6 by O_2, leading to an improvement of the efficiency of CO and C_3H_6 utilization for NO reduction. Catalyst characterizations such as H_2-TPR and X-ray absorption spectroscopy (XANES and EXAFS) revealed that Rh species in the Ir-Rh/CeO_2-ZrO_2 samples is mainly present as Rh_2O_3 nanoparticles and the addition of small amount of Ir (Ir/Rh = 1/9) can improve the reducibility of Rh_2O_3 nanoparticles. On the basis of surface analysis by XPS, FT-IR spectroscopy following CO adsorption and STEM observation, the formation of Ir-Rh nanoparticles composed of finely-divided Ir species on the surface of Rh particles with a size of 1 nm was considered to be responsible for high catalytic activity of Ir-Rh/CeO_2-ZrO_2 for NO-CO-C_3H_6-H_2-O_2 reaction. Ir-Rh/CeO_2-ZrO_2 with Ir-Rh loading of 0.3 wt% showed still high catalytic performance, which is comparable with that of 0.5 wt% Rh/CeO_2-ZrO_2, leading to minimize the Rh usage.

Introduction

Three-way catalysts (TWCs) represent one of the most innovative technologies for automotive emission control. TWCs can work simultaneously and efficiently to reduce NO and to oxidize CO and hydrocarbons at the theoretical air/fuel (A/F) ratio of around 14.6. The catalytically active components in TWCs are platinum group metals (PGMs), such as platinum, palladium and rhodium, although oxygen storage materials such as CeO_2-ZrO_2 mixed oxides, which can widen the operational A/F window, are key components in TWCs.[1] The total demand for PGMs for automotive catalysts is growing due to increasing environmentally awareness. Among them, Rh is the scarcest, and more than 80% of the world Rh demand is for use in TWCs.[2] This is because Rh is the primary constituent in all TWCs for controlling NOx emission.[3,4] Studies to minimize the use of Rh are gaining extensive attention as a result.[5,6]

Improving the intrinsic performance of TWCs is the most important approach to develop highly active catalysts with low PGM loading. Extensive research and development has been performed for this purpose, and for example, the performance of TWCs has been improved by the addition of many kinds of promoters. Kawabata *et al.*[7,8] investigated the additive effect of lanthanoid (La, Ce, Pr or Nd) on the catalytic performance of Rh/ZrO_2 – TWC, and found that Rh catalyst supported on La-containing ZrO_2 showed high performance for the removal of NO*x* and hydrocarbons. They explained the high catalytic activity of Rh/La-ZrO_2 by the stabilization of Rh species in low oxidation state during the three-way catalytic reaction. Tanabe *et al.*[9] reported that Rh can interact strongly with Nd_2O_3, resulting in Rh sintering suppression by the formation of Rh-O-Nd bond. However, the anchoring effect with adequate Nd_2O_3 was pointed out to cause a lowering of the reducibility of Rh species.

On the other hand, Machida *et al.*[10] proposed an importance of realization of optimum Rh – support interactions to develop highly active catalysts with minimized Rh loading. They extensively investigated the catalytic performance of Rh catalysts supported on various metal phosphate materials, which possess relatively high thermal stability, and reported that Rh/tridymite-$AlPO_4$ showed the highest catalytic activity for NO-CO-C_3H_6-O_2 reactions after high-temperature ageing.[11] High thermal stability of Rh species was accounted for by the creation of metal – support interaction via a Rh – O – P bond, and the highly dispersed Rh species interacting with $AlPO_4$ can be easily reduced by the reaction gas because of weak Rh – O – P bond, resulting in high catalytic activity.[12] We have recently reported that the catalytic activity of Rh supported on Y-stabilized ZrO_2 for NO-CO-C_3H_6-O_2 reaction under a stoichiometric condition is effectively improved by addition of small amount of CeO_2 (5 mol%).[13] This improvement was ascribed to the formation of easily reducible Rh species by interacting with a Ce-Zr solid solution on the basis of TEM, H_2-TPR and FT-IR spectroscopy following CO adsorption. Although ceria-based oxide is known to be not suitable support oxide for Rh because of the formation of stable Rh species in the oxide state,[14,15] the catalyst design to stabilize Rh in active state and to make good use of the redox function of ceria-based oxide is an important issue.[16-19]

Bimetallic alloy systems have been extensively studied to improve the intrinsic performance of TWCs, leading to a minimum use of PGMs. Vedyagin *et al.*[20] investigated the catalytic performance of Pd-Rh alloyed catalysts supported on Al_2O_3 for three-way catalytic reactions, and found that the bimetallic Pd-Rh catalysts showed higher activity than the monometallic catalysts after high-temperature ageing. This suggests that the combination of Rh and Pd leads to superior thermal stability. Renème *et al.*[21] revealed that the kinetics in NO/H_2 reaction on Pd/Al_2O_3 is altered by addition of Rh. The predominant H_2/O_2 reaction on Pd/Al_2O_3 depletes the surface hydrogen inducing the dissociation of NO on a nearest-neighbor vacant sites, suggesting a competitive adsorption of NO and H_2/O_2. The dissociation of NO preferentially occurs on Rh sites in bimetallic $Pd\text{-}Rh/Al_2O_3$, resulting in none competitive adsorption process. A synergistic Pt-Rh bimetallic catalysts supported on Al_2O_3 has also been reported to show superior performance for NO/H_2 reaction.[22]

It is well known that Pt and Pd can strongly adsorb CO, which is one of the major pollutants emitted from gasoline engines, leading to the inhibition of important reaction steps such as NO reduction and HC oxidation in three-way catalytic reaction. In case of bimetallic catalysts including Pt and Pd, CO molecule seems to be preferentially adsorbed on Pt and Pd.[23,24] Therefore, the combination of Rh with another metal, which does not cause the reaction inhibition by CO, would be an important strategy to improve the intrinsic performance of TWCs. Among the PGMs, Ir has been reported to show unique catalytic property for NO reduction by CO in the presence and absence of O_2.[25,26] We have also found that Ir/SiO_2 – based catalysts show excellent catalytic activity for the selective reduction of NO with CO in the presence of excess oxygen.[27,28] Fujitani *et al.*[29,30] intensively investigated the adsorption behavior and reaction properties of NO and CO on Ir(111), and found that CO species preadsorbed on Ir(111) does not affect the adsorption of NO on hollow sites, indicating the presence of independent adsorption sites for CO and NO on Ir surface. Similar adsorptive properties of Ir have also been proposed by Chen *et al.*[31] Ir would be thus a good candidate as additive component in Rh – TWCs for NOx removal.

In the present work, we have investigated the catalytic performance of bimetallic Ir-Rh catalysts supported on $CeO_2\text{-}ZrO_2$ for $NO\text{-}CO\text{-}C_3H_6\text{-}H_2\text{-}O_2$ reaction in a stoichiometric condition. Since Ir/CeO_2 shows excellent activity for NO reduction with C_3H_6 in a stoichiometric condition,[32] the essential role of Ir in promoting NO conversion is discussed based on the reaction data as well as catalyst characterizations such as temperature-programmed reduction by H_2 (H_2-TPR), X-ray absorption spectroscopy (XANES and EXAFS), X-ray photoelectron spectroscopy (XPS) and Fourier transform infrared (FT-IR) spectroscopy following CO adsorption.

Experimental

Catalyst preparation

$CeO_2\text{-}ZrO_2$ mixed oxide with the Ce/Zr molar ratio of 1/4 was prepared using a coprecipitation method using ammonium cerium(IV) nitrate (Wako Pure Chemical Industries) and zirconium(IV) oxynitrate (Wako Pure Chemical Industries) as precursor. To a solution of cerium and zirconium precursors was added an aqueous solution of ammonia as a precipitation agent at room temperature. The precipitate thus obtained was washed with distilled water, dried at 110 °C and then calcined at 800 °C for 3 h in air. The resulting $CeO_2\text{-}ZrO_2$ powder was then impregnated with a solution of $Rh(NO_3)_3$ (Ishifuku Metal Industry; Rh: 4.46 wt% in solution) and $Ir(NO_3)_4$ (Ishifuku Metal Industry; Ir: 7.91 wt% in solution), followed by drying at 110 ºC overnight and calcination at 600 ºC for 3 h in air. The Ir/Rh atomic ratio was changed as follows: Ir/Rh = 0/1, 1/9, 1/4, 1/1, 4/1, 1/0. The total loading of Ir + Rh was fixed at 0.5 wt% unless otherwise specified.

Structural characterization

The BET surface area of the catalysts was determined by N_2 physisorption at liquid nitrogen temperature using Micromeritics ASAP 2010, after evacuating the samples at 200 ºC for 1 h. X-ray diffraction (XRD) patterns were recorded using a Rigaku MiniFlex diffractometer with Cu Kα radiation at 30 kV and 15mA. The scanning was done from $2\theta = 20 - 60$ º at a speed of 1 deg min^{-1}. The XPS analyses were performed with a ULVAC-PHI PHI-5000 using a monochromated Al Kα radiation ($h\nu$ = 1486.6 eV). The binding energy was corrected by the contaminated carbon (284.6 eV). The local structures around Rh ions were studied by measuring the Rh K-edge X-ray absorption spectra using the BL-14B2 at the SPring-8 facility (Hyogo, Japan) with a ring energy of 8.0 GeV and a stored current of 100 mA. XAFS spectra were recorded in a fluorescent mode at room temperature with a Si(311) channel cut monochromator. STEM images were obtained with a JEM-ARM200F (JEOL), operating at the acceleration voltage of 200 kV. The elemental analysis was performed by combining STEM/HAADF images with EDS (EDAX Inc.).

Dispersion and reducibility of Rh-Ir

The dispersion of Ir-Rh was calculated from CO chemisorption measured by the pulse method at room temperature, in which the sample was first reduced with H_2 at 400 ºC for 1 h and then cooled to room temperature in flowing He. H_2-TPR measurement was conducted to estimate the reducibility of the catalysts. The TPR profiles were obtained from room temperature to 600 °C in a 30 cm^3min^{-1} flow of 5% H_2/Ar at a heating rate of 10 °C min^{-1}. The consumption of H_2 was monitored using a thermal conductivity detector (TCD).

Infrared spectroscopy

FT-IR spectra of adsorbed CO species were taken with a JASCO FT/IR 4200 spectrometer at a resolution of 4 cm^{-1} under a static condition. Prior to each experiment, a self-supporting sample disk (14 $mg \cdot cm^{-2}$) was placed in an IR cell with CaF_2 windows, pretreated with hydrogen at 40.0 kPa for 1 h, and then evacuated at 400 ºC for 2 h. The background spectrum of the treated surface was measured for spectral correction at room temperature. Observation of surface species was carried out after introduction of CO at 6.67 kPa at room temperature.

Catalytic activity measurement

Catalytic activity was evaluated using a fixed-bed continuous flow reactor. A sample of the catalyst (0.1 g) was held in a quartz tube (10 mm i.d.) by packing quartz wool at both ends of the catalyst bed. Prior to each reaction, the catalyst was pretreated in the flow of 1% H_2/N_2 at 400 °C for 1 h. The reaction gas was a stoichiometric mixture of 0.1% NO, 400 ppm C_3H_6, 0.3% CO, 0.1% H_2, 0.33% O_2, 2% H_2O and the balance comprising N_2. The flow rate of the reaction gas was 500 cm^3min^{-1}, which corresponds to 250,000 h^{-1} in GHSV. The catalytic activity was measured while raising the temperature from 40 to 600 °C at a rate of 4 °C min^{-1}. The concentrations of NO*x*, O_2, CO and CO_2 and the total hydrocarbons in the effluent gas were continuously monitored using an on-line gas analyzer, Horiba, PG-240 and Shimadzu, VMS-1000F, respectively.

Results and discussion

Physico-chemical properties of Ir-Rh/CeO_2-ZrO_2

Table 1 summarizes the BET surface area of and the dispersion of Ir-Rh in Ir-Rh/CeO_2-ZrO_2 samples. Although the BET surface area of CeO_2-ZrO_2 was slightly decreased by addition of Rh and Ir, no significant difference was observed for Ir-Rh/CeO_2-ZrO_2 with different Ir/Rh ratio. The dispersion of Ir-Rh was found to be monotonously decreased when Ir was added to Rh.

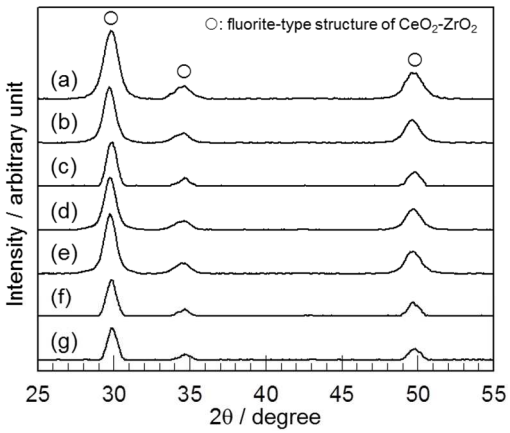

Fig. 1 XRD patterns of (a) CeO_2-ZrO_2, (b) Rh/CeO_2-ZrO_2 (Ir/Rh=0/1), (c) Ir-Rh/CeO_2-ZrO_2 (Ir/Rh=1/9), (d) Ir-Rh/CeO_2-ZrO_2 (Ir/Rh=1/4), (e) Ir-Rh/CeO_2-ZrO_2 (Ir/Rh=1/1), (f) Ir-Rh/CeO_2-ZrO_2 (Ir/Rh=4/1) and (g) Ir/CeO_2-ZrO_2 (Ir/Rh=1/0).

Fig. 1 shows the XRD patterns of Ir-Rh/CeO_2-ZrO_2 samples. It was verified that CeO_2-ZrO_2 possesses a fluorite-type structure despite a large amount of zirconium, indicating the formation of solid solution. This is in good agreement with our previous reports.[33] The addition of Ir and Rh into CeO_2-ZrO_2 did not cause a change in their XRD patterns, suggesting no structural change of CeO_2-ZrO_2. It is also noteworthy that XRD peaks ascribed to Ir and Rh species were not detected in the XRD patterns of Ir-Rh/CeO_2-ZrO_2 irrespective of Ir/Rh ratios. This is probably due to high dispersion state of Ir-Rh species and its low content.

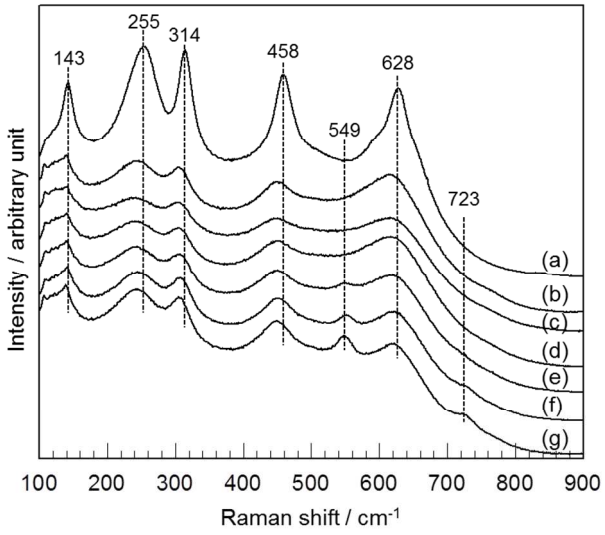

Fig. 2 Raman spectra of (a) CeO_2-ZrO_2, (b) Rh/CeO_2-ZrO_2 (Ir/Rh=0/1), (c) Ir-Rh/CeO_2-ZrO_2 (Ir/Rh=1/9), (d) Ir-Rh/CeO_2-ZrO_2 (Ir/Rh=1/4), (e) Ir-Rh/CeO_2-ZrO_2 (Ir/Rh=1/1), (f) Ir-Rh/CeO_2-ZrO_2 (Ir/Rh=4/1) and (g) Ir/CeO_2-ZrO_2 (Ir/Rh=1/0).

In order to obtain information on the structure of CeO_2-ZrO_2, Ir and Rh species, Raman spectra of Ir-Rh/CeO_2-ZrO_2 were measured, because Raman spectroscopy is a more sensitive method for identifying changes in M–O bond arrangement. As shown in Fig. 2(a), five distinct Raman bands were detected at 143, 255, 314, 458 and 628 cm^{-1} in the Raman spectrum of CeO_2-ZrO_2, which are characteristic of the tetragonal phase.[34-36] Although CeO_2-ZrO_2 was suggested to possess a fluorite-type structure by XRD, Raman spectroscopy revealed the presence of tetragonal phase as crystal structure of CeO_2-ZrO_2. It appears that no significant difference in the Raman spectra of Ir-Rh/CeO_2-ZrO_2 was observed, indicating that Rh and Ir do not affect the crystal structure of CeO_2-ZrO_2. When Ir content was increased up to the Ir/Rh ratio of 1/1, weak but

Table 1. BET surface area and Ir-Rh dispersion for Ir-Rh/CeO_2-ZrO_2.

Catalyst	Rh (wt%)	Ir (wt%)	BET surface area (m^2g^{-1})	Ir-Rh dispersion (CO/IrRh)
CeO_2-ZrO_2	0.00	0.00	63.9	---
Rh/CeO_2-ZrO_2 (Ir/Rh=0/1)	0.50	0.00	62.9	0.83
Ir-Rh/CeO_2-ZrO_2 (Ir/Rh=1/9)	0.41	0.09	61.5	0.76
Ir-Rh/CeO_2-ZrO_2 (Ir/Rh=1/4)	0.34	0.16	62.8	0.62
Ir-Rh/CeO_2-ZrO_2 (Ir/Rh=1/1)	0.17	0.33	60.7	0.38
Ir-Rh/CeO_2-ZrO_2 (Ir/Rh=4/1)	0.06	0.44	60.2	0.16
Ir/CeO_2-ZrO_2 (Ir/Rh=1/0)	0.00	0.50	60.7	0.09

distinct bands were detected at 549 and 723 cm^{-1}, which can be assigned to IrO_2.[37,38] The intensity of these bands increased with increasing Ir content. This indicates that iridium is present as IrO_2 in the catalyst. On the other hand, no Raman bands ascribed to RhOx species, which are reported to be detected at ~540 cm^{-1},[39] were observed in the Raman spectra of Ir-Rh/CeO_2-ZrO_2. In accordance with the results of Rh dispersion given in Table 1, Rh species are expected to be highly dispersed on the surface of CeO_2-ZrO_2.

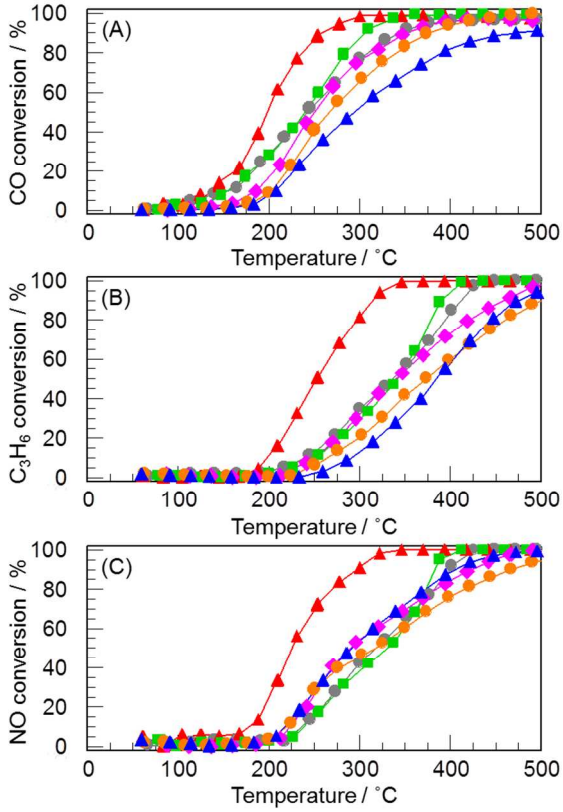

Fig. 3 Change in (A) CO conversion, (B) C_3H_6 conversion and (C) NO conversion as a function of temperature for NO-CO-C_3H_6-H_2-O_2 reaction over Rh/CeO_2-ZrO_2 (Ir/Rh=0/1) (●), Ir-Rh/CeO_2-ZrO_2 (Ir/Rh=1/9) (▲), Ir-Rh/CeO_2-ZrO_2 (Ir/Rh=1/4) (■), Ir-Rh/CeO_2-ZrO_2 (Ir/Rh=1/1) (◆), Ir-Rh/CeO_2-ZrO_2 (Ir/Rh=4/1) (●) and Ir/CeO_2-ZrO_2 (Ir/Rh=1/0) (▲).

Catalytic activity of Ir-Rh/CeO_2-ZrO_2

Fig. 3 shows the temperature dependence of conversion efficiencies of NO, CO and C_3H_6 over Ir-Rh/CeO_2-ZrO_2 with different Ir/Rh ratio, which was reduced at 400 ºC as pretreatment, for NO-CO-C_3H_6-H_2-O_2 reaction. It seems that the oxidation of CO and C_3H_6 and the reduction of NO simultaneously take place on Ir-Rh/CeO_2-ZrO_2 in the entire temperature range. This is in accordance with previous reports in which the catalytic activity of supported Rh catalysts for simulated stoichiometric exhaust gas containing NO, CO, C_3H_6 and O_2 has been evaluated.[10,11,13] As can be seen in Fig. 3, it is of interest that the addition of a small amount of Ir caused a significant increase in not only CO and C_3H_6 oxidation activity but also NO reduction activity, indicating that Ir additive can improve the TWC activity of Rh catalysts. The highest TWC activity was achieved on Ir-Rh/CeO_2-ZrO_2 with Ir/Rh atomic ratio of 1/9. It should be noted that the presence of excess amount of Ir additive caused a decrease in the TWC activity of Rh catalysts.

As can be seen in Figs. 3(A) and (B), CO and C_3H_6 oxidation activity of Ir-Rh/CeO_2-ZrO_2 with higher Ir/Rh atomic ratio was monotonously decreased with increasing Ir content. On the other hand, no significant difference in the NO reduction activity of Ir-Rh/CeO_2-ZrO_2 with higher Ir/Rh atomic ratio was observed. These results suggest that Ir additive can alter the efficiency of CO and C_3H_6 utilization for NO reduction, which means the reaction selectivity of NO, CO and C_3H_6 molecules, on Rh/CeO_2-ZrO_2. In order to confirm this idea, the efficiency of CO and C_3H_6 utilization was defined as the ratio of "number of reduced NO molecules" toward "number of oxidized CO and C_3H_6 molecules". Here, the efficiency of H_2 utilization was excluded, because the concentration of H_2 in the reaction gas was not measured by on-line gas analyser employed in this study. In addition, we have observed no significant difference in NO conversion on Rh/CeO_2-ZrO_2 and Ir-Rh/CeO_2-ZrO_2 (Ir/Rh=1/9) in the absence and presence of H_2 in another set of experiment, suggesting that H_2 does not directly act as reducing agent for the reduction of NO. Fig. 4 shows the efficiency of CO and C_3H_6 utilization for NO reduction on Ir-Rh/CeO_2-ZrO_2 thus estimated. It appears that Ir/CeO_2-ZrO_2 gave relatively high efficiency of CO and C_3H_6 utilization compared with Rh/CeO_2-ZrO_2, indicating that Ir additive can suppress the preferential oxidation of CO and C_3H_6 by O_2. In fact, the efficiency of CO and C_3H_6 utilization for Ir-Rh/CeO_2-ZrO_2 was higher than that for Rh/CeO_2-ZrO_2 and lower than that of Ir/CeO_2-ZrO_2.

Although the dispersion of Ir-Rh was monotonously decreased when Ir was added to Rh (Table 1), the highest TWC activity was achieved on Ir-Rh/CeO_2-ZrO_2 with Ir/Rh atomic ratio of 1/9. Taking into account the fact that Rh/CeO_2-ZrO_2 showed higher TWC activity than Ir/CeO_2-ZrO_2, Rh species can be considered to be the catalytically active component. Therefore, Ir additive is suspected to affect the chemical state of Rh species, resulting in the improvement of catalytic performance. Effect of Ir additive on the chemical state of Rh species will be discussed below.

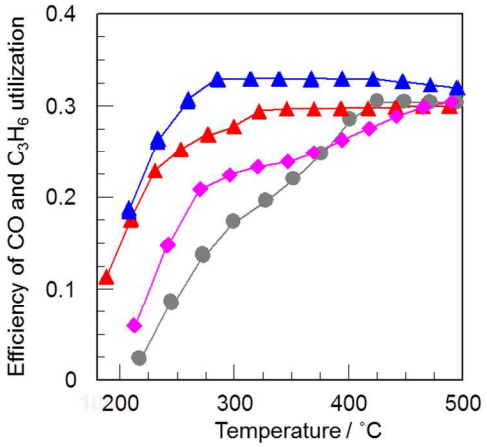

Fig. 4 Efficiency of CO and C_3H_6 utilization for NO reduction on over Rh/CeO_2-ZrO_2 (Ir/Rh=0/1) (●), Ir-Rh/CeO_2-ZrO_2 (Ir/Rh=1/9) (▲), Ir-Rh/CeO_2-ZrO_2 (Ir/Rh=1/1) (◆) and Ir/CeO_2-ZrO_2 (Ir/Rh=1/0) (▲).

Reducibility of Ir-Rh species by H_2-TPR

Fig. 5 shows H_2-TPR profiles of Ir-Rh/CeO_2-ZrO_2 with different Ir/Rh ratio. Very broad H_2 consumption peak was observed for CeO_2-ZrO_2 in the temperature range above 500 ºC. Rh/CeO_2-ZrO_2 and Ir/CeO_2-ZrO_2 gave H_2 consumption peak at 98 and 161 ºC, respectively, which can be ascribed to the reduction of Rh oxide[5,9,40-42] and Ir oxide species,[28,32] and/or their interface with CeO_2-ZrO_2. It is noteworthy that the reducibility of Rh species supported on CeO_2-ZrO_2 is quite different depending on the amount of Ir additive. When a small amount of Ir was added to Rh/CeO_2-ZrO_2 (Ir/Rh=1/9), a shift of the H_2 consumption peak from 98 to 90 ºC was observed, indicating that the addition of a small amount of Ir can improve the reducibility of Rh species. However, further increase in Ir additive caused a shift of H_2 consumption peak to higher temperature.

It should be noted that Ir-Rh/CeO_2-ZrO_2 gave one H_2 consumption peak in the H_2-TPR profile. If Rh and Ir oxide species are independently present on the surface of CeO_2-ZrO_2, two peaks at around 98 and 161 ºC attributed to the reduction of Rh oxide and Ir oxide species must be observed. Therefore, it can be expected the creation of intimate contact of Rh species with Ir species, suggesting the uniform dispersion of Ir species on Rh particles or *vice versa*.

Valence state of Rh species after H_2 treatment by XAFS and XPS

The creation of intimate contact of Rh species with Ir species would lead us to consideration that the surface valence state of Rh particles interacted with Ir species in Ir-Rh/CeO_2-ZrO_2 is different from that of Rh particles supported on CeO_2-ZrO_2. In order to verify this hypothesis, X-ray absorption measurements were performed for Rh/CeO_2-ZrO_2 and Ir-Rh/CeO_2-ZrO_2 with Ir/Rh = 1/9. Here, the samples were reduced in the flow of 1% H_2/N_2 at 400 °C for 1 h as pretreatment, because the reducibility of Rh species in the latter catalyst was quite high (Fig. 5) and the pre-reduced latter catalyst showed the highest TWC activity (Fig. 3).

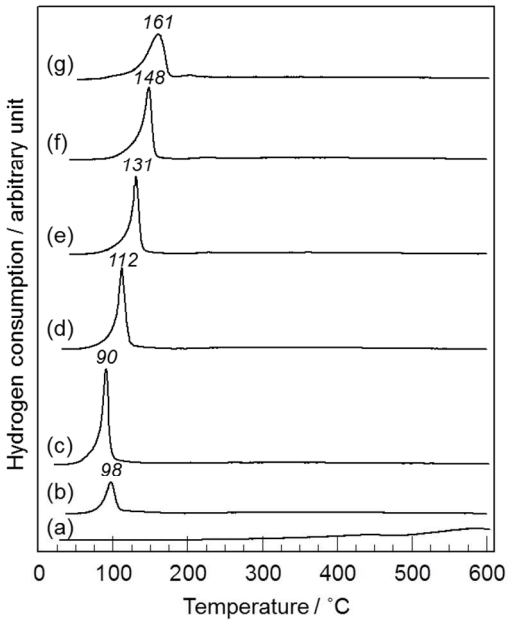

Fig. 5 H_2-TPR profiles of (a) CeO_2-ZrO_2, (b) Rh/CeO_2-ZrO_2 (Ir/Rh=0/1), (c) Ir-Rh/CeO_2-ZrO_2 (Ir/Rh=1/9), (d) Ir-Rh/CeO_2-ZrO_2 (Ir/Rh=1/4), (e) Ir-Rh/CeO_2-ZrO_2 (Ir/Rh=1/1), (f) Ir-Rh/CeO_2-ZrO_2 (Ir/Rh=4/1) and (g) Ir/CeO_2-ZrO_2 (Ir/Rh=1/0).

Fig. 6(A) shows Rh K-edge XANES (X-ray absorption near edge structure) spectra of Rh/CeO_2-ZrO_2 and Ir-Rh/CeO_2-ZrO_2 with Ir/Rh = 1/9 after the reduction treatment at 400 °C together with that of pure Rh foil and Rh_2O_3 as reference sample. The XANES spectra of Rh/CeO_2-ZrO_2 and Ir-Rh/CeO_2-ZrO_2 were very similar to that of Rh_2O_3, indicating that Rh is present in the +3 oxidation state irrespective of Ir additive. Fig. 6(B) shows Fourier transforms of the k^3-weighted EXAFS (extended X-ray absorption fine structure) spectra, phase-shift uncorrected, of Rh/CeO_2-ZrO_2, Ir-Rh/CeO_2-

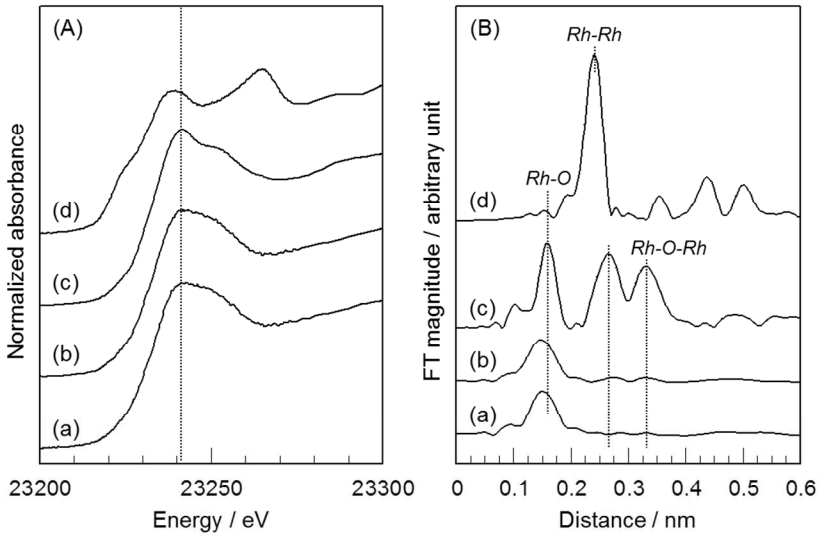

Fig. 6 (A) Rh K-edge XANES and (B) Fourier transforms EXAFS spectra of (a) Rh/CeO_2-ZrO_2 (Ir/Rh=0/1) and (b) Ir-Rh/CeO_2-ZrO_2 (Ir/Rh=1/9) after the reduction treatment at 400 °C and (c) Rh_2O_3 and (d) Rh foil.

ZrO_2 and two references (Rh foil and Rh_2O_3). Rh/CeO_2-ZrO_2 and Ir-Rh/CeO_2-ZrO_2 with Ir/Rh = 1/9 showed the peak at around 0.16 nm, which is attributed to a Rh – O shell.[12,43] However, the second (Rh – Rh) and third shells (Rh – O – Rh) were not observed. These results suggest that Rh species in the samples is mainly present as Rh_2O_3 nanoparticles.

In order to gain information on the surface electric state of Rh, XPS measurements were performed for Rh/CeO_2-ZrO_2 and Ir-Rh/CeO_2-ZrO_2 with Ir/Rh = 1/9 before and after the reduction treatment at 400 °C. Fig. 7 shows the XPS spectra of Ir-Rh/CeO_2-ZrO_2 samples in the Rh 3d region. The peak of the Rh $3d_{5/2}$ binding energy for the samples without reduction treatment appeared at around 309.2 eV, the value of which is in agreement with the reference data for Rh_2O_3.[43] This indicates that the surface of Rh species in the Ir-Rh/CeO_2-ZrO_2 samples without reduction treatment is stabilized in the +3 oxidation state irrespective of Ir additive. When Ir-Rh/CeO_2-ZrO_2 sample was reduced with H_2 at 400 °C, in addition to Rh^{3+} species, the Rh $3d_{5/2}$ peak ascribed to Rh^0 was also detected at around 308.1 eV. The peak area ratio, $A_{308.1\ eV}/A_{309.2\ eV}$, was found to be 0.581 and 0.754 for Rh/CeO_2-ZrO_2 and Ir-Rh/CeO_2-ZrO_2, respectively, indicating that the latter sample contains relatively larger amount of Rh^0 species than the former one. In accordance with the results of H_2-TPR, the addition of a small amount of Ir can improve the reducibility of Rh species.

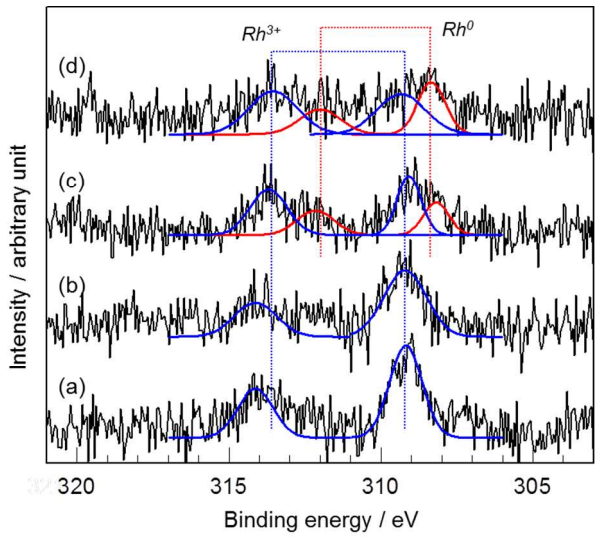

Fig. 7 Rh 3d XPS spectra of (a), (c) Rh/CeO_2-ZrO_2 (Ir/Rh=0/1) and (b), (d) Ir-Rh/CeO_2-ZrO_2 (Ir/Rh=1/9). Here, (a), (b) the samples as prepared and (c), (d) the samples after the reduction treatment at 400 °C.

Surface chemical state of Ir-Rh species by FT-IR following CO adsorption

Surface chemical state of Ir-Rh species supported on CeO_2-ZrO_2 was investigated by measuring FT-IR spectra of CO species adsorbed on Ir-Rh/CeO_2-ZrO_2 samples reduced at 400 °C. As can be seen in Fig. 8(a), exposure of CO to Rh/CeO_2-ZrO_2, followed by evacuation at room temperature, gave distinct IR bands due to a gem-dicarbonyl species on Rh^+ $(Rh^+(CO)_2)$[44-46] at 2018 and 2085 cm^{-1} and a linearly bonded CO species on Rh^0 $(Rh^0\text{-}CO)$[47-79] at 2055 cm^{-1}. Raskó *et al.*[50] and Cavanagh *et al.*[51] reported that the appearance of the bands due to gem-dicarbonyl and linearly bonded CO species depends on the Rh content in Rh/Al_2O_3 sample. The IR band due to linearly bonded CO species is favourable in case of Rh/Al_2O_3 with higher Rh content. This was ascribed to the formation of three dimensional Rh_x crystallites in which there are Rh^0 atoms surrounded only by Rh^0 atoms. Therefore, Rh species supported on CeO_2-ZrO_2 prepared in this study are presumed to be present as three dimensional Rh_x crystallites. When CO was adsorbed on Ir-CeO_2-ZrO_2 (Fig. 8(f)), in accordance with literature,[27,52-54] the IR band assignable to CO species linearly bonded on Ir^0 at 2081 cm^{-1} was observed.

As can be seen in Figs. 8(b)-(d), CO adsorption on Ir-Rh/CeO_2-ZrO_2 with Ir/Rh = 1/9, 1/4 and 1/1 gave rise to completely different IR spectrum from that for Rh/CeO_2-ZrO_2 and Ir-CeO_2-ZrO_2. Strong IR band due to CO species linearly bonded on Rh^0 at 2035 cm^{-1} along with those of shoulder bands at 2018 and 2085 cm^{-1} which can be due to gem-dicarbonyl species was clearly observed, although the band intensity was decreased with Ir content because of a decrease in the Ir-Rh dispersion (Table 1). It should be noted that the addition of Ir into Rh/CeO_2-ZrO_2 caused a significant shift of IR band due to Rh^0-CO from 2055 to 2035 cm^{-1}. These results suggest that not only the surface electric state of Rh species but also the surface morphology of Rh particles were drastically modified by Ir additive.

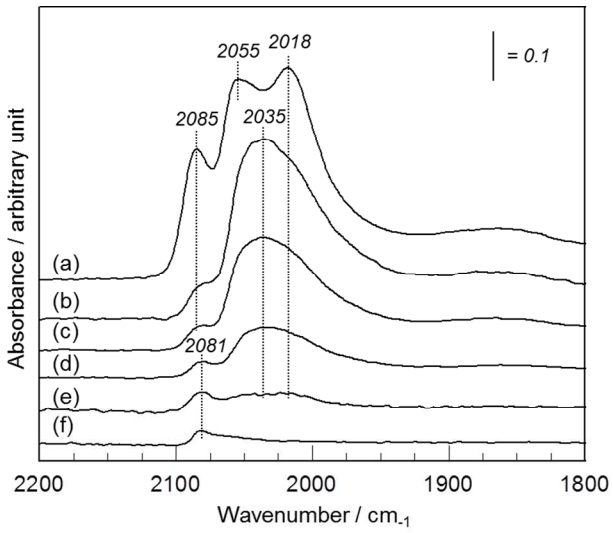

Fig. 8 FT-IR spectra of CO species adsorbed remaining on (a) Rh/CeO_2-ZrO_2 (Ir/Rh=0/1), (b) Ir-Rh/CeO_2-ZrO_2 (Ir/Rh=1/9), (c) Ir-Rh/CeO_2-ZrO_2 (Ir/Rh=1/4), (d) Ir-Rh/CeO_2-ZrO_2 (Ir/Rh=1/1), (e) Ir-Rh/CeO_2-ZrO_2 (Ir/Rh=4/1) and (f) Ir/CeO_2-ZrO_2 (Ir/Rh=1/0) after evacuation at room temperature.

Presumed surface state of Rh particles in Ir-Rh/CeO_2-ZrO_2

As can be seen in Fig. 6(B), no peaks ascribed to the presence of Rh – Ir bonding was observed in the EXAFS spectrum of Ir-Rh/CeO_2-ZrO_2 sample with Ir/Rh = 1/9, which showed the highest TWC activity (Fig. 4). This suggests that the alloyed Ir-Rh particles were not formed in the Ir-Rh/CeO_2-ZrO_2 sample. On the other hand, the finding that one H_2 consumption peak was observed in the H_2-TPR

profile of Ir-Rh/CeO_2-ZrO_2 with various Ir/Rh atomic ratios (Fig. 5) clearly suggests that Rh nanoparticles are strongly interacted with Ir species, resulting in the uniform dispersion of Ir species on Rh particles or *vice versa*.

FT-IR spectroscopy following CO adsorption revealed that not only the surface electric state of Rh species but also the surface morphology of Rh particles were drastically modified by Ir additive (Fig. 8). Namely, strong IR band due to CO species linearly bonded on Rh^0 was predominantly observed for Ir-Rh/CeO_2-ZrO_2, whereas the IR bands due to $Rh^+(CO)_2$ were main peaks in the IR spectrum for Rh/CeO_2-ZrO_2. Similar change in the IR spectra observed for single and bimetallic samples has been reported by Van Slooten and Nieuwenhuys.[55] They measured the FT-IR spectra of CO species adsorbed on Pt/SiO_2, Rh/SiO_2 and Pt-Rh/SiO_2, and observed a shift of IR band due to CO species linearly coordinated to Pt or Rh and a disappearance of gem-dicarbonyl bands for Pt-Rh/SiO_2. They concluded that Pt-Rh/SiO_2 catalyst does not contain isolated Rh atoms and, hence, that the Rh atoms are present in alloy particles. In the present study, the IR spectra observed for IrRh/CeO_2-ZrO_2 was found to be completely different from that for Rh/CeO_2-ZrO_2 (Fig. 8), suggesting the absence of isolated Rh particles in the Ir-Rh/CeO_2-ZrO_2 samples. No change in the characteristics of IR spectra for Ir-Rh/CeO_2-ZrO_2 was also observed when Ir/Rh atomic ratio was changed from 1/9 to 1/1.

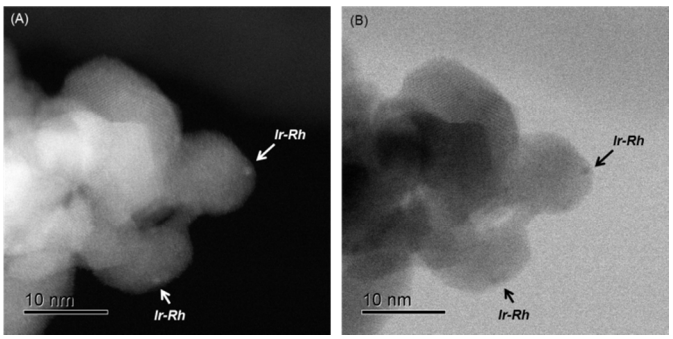

Fig. 9 (A) STEM/HAADF and (B) STEM/BF images of Ir-Rh/CeO_2-ZrO_2 (Ir/Rh=1/9) after the reduction treatment at 400 °C.

STEM and EDS analyses revealed that Ir-Rh particle were highly dispersed with a size of 1 nm over the surface of CeO_2-ZrO_2 (Fig. 9 and Fig. S1 in ESI† for the elemental analysis of the nanoparticles). Taking into account the fact that the amount of Rh atoms in the catalyst is higher than that of Ir atoms, the formation of Ir-Rh nanoparticles composed of finely-divided Ir species on the surface of Rh particles can be considered. This would be responsible for high catalytic activity of IrRh/CeO_2-ZrO_2 with Ir/Rh atomic ratio of 1/9. It is also noteworthy that Ir-Rh/CeO_2-ZrO_2 with Ir/Rh atomic ratio of 1/9 showed higher efficiency of CO and C_3H_6 utilization for NO reduction than that with Ir/Rh = 1/1 (Fig. 4). Such high efficiency of CO and C_3H_6 utilization would also be related to the strong interaction between finely-divided Ir species and Rh particles. When Ir content was increased up to the Ir/Rh atomic ratio of 1/1, the presence of small particles composed of Ir and Rh species was also recognized by STEM and EDS analyses (Fig. S2 in ESI† for the elemental analysis of the nanoparticles). However, as summarized in Table 1, the Ir-Rh dispersion estimated from the amount of CO chemisorption was clearly decreased with increasing the Ir content. Therefore, slightly agglomerated Ir particles are suspected to interact with Rh particles, leading to a decrease of TWC performance including activity and selectivity.

Effect of Ir-Rh loading on the TWC activity of Ir-Rh/CeO_2-ZrO_2

Because the studies of ways to lessen the amount of Rh usage in automotive catalysts are important issue from practical point of view, the effect of IrRh loading on the TWC activity of Ir-Rh/CeO_2-ZrO_2 with Ir/Rh = 1/9, which showed the highest activity, was examined. Fig. 10 shows the relationship between the Ir-Rh loading and the light-off temperature, $T_{50\%}$, at which the conversion reaches 50%, for Ir-Rh/CeO_2-ZrO_2 along with the $T_{50\%}$ value for 0.5 wt% Rh/CeO_2-ZrO_2. It appears that the $T_{50\%}$ value was increased with decreasing Ir-Rh loading, indicating the decrease in the TWC performance. However, the threshold Ir-Rh loading at which the $T_{50\%}$ value is steeply risen is slightly different for CO and C_3H_6 oxidation and NO reduction. Namely, the threshold Ir-Rh loading for NO reduction is 0.3 wt%, while that for C_3H_6 oxidation is 0.4 wt%. In case of CO oxidation, the $T_{50\%}$ value was gradually increased with Ir-Rh loading. As given in Fig. 10, the $T_{50\%}$ values for CO and C_3H_6 oxidation and NO reduction on 0.5 wt% Rh/CeO_2-ZrO_2 were found to be 242, 337 and 318 °C, respectively. The TWC performance of 0.3 wt% Ir-Rh/CeO_2-ZrO_2 seems to be comparable with that of 0.5 wt% Rh/CeO_2-ZrO_2. Therefore, Ir-Rh/CeO_2-ZrO_2 is effective catalyst leading to minimize the Rh usage.

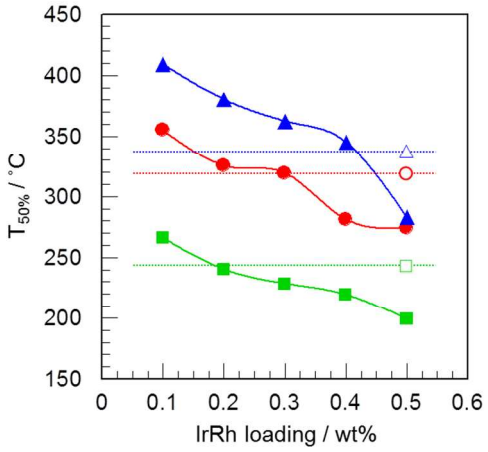

Fig. 10 Change in the light-off temperature ($T_{50\%}$) of CO conversion (■,□), C_3H_6 conversion (▲,△) and NO conversion (●,○) over Ir-Rh/CeO_2-ZrO_2 (Ir/Rh=1/9) (■,▲,●) and 0.5 wt% Rh/CeO_2-ZrO_2 (Ir/Rh=0/1) (□,△,○) as a function of Ir-Rh loading.

Conclusions

The effect of Ir additive on the catalytic performance of Rh/CeO_2-ZrO_2 with the Ce/Zr molar ratio of 1/4 for NO-CO-C_3H_6-H_2-O_2 reaction in a stoichiometric condition was investigated. The dispersion of Ir-Rh estimated by CO chemisorption method was monotonously decreased with increasing the Ir content.

Nevertheless, the catalytic activity of Rh/CeO_2-ZrO_2 for three-way catalytic reactions (CO and C_3H_6 oxidation and NO reduction) was significantly improved by addition of a small amount of Ir. The optimum Ir/Rh atomic ratio was 1/9. Ir additive was found to increase the efficiency of CO and C_3H_6 utilization for NO reduction, which means the reaction selectivity of NO, CO and C_3H_6 molecules, on Rh/CeO_2-ZrO_2.

H_2-TPR measurements exhibited that H_2 consumption peak due to the reduction of Rh species was clearly lowered by addition of Ir with Ir/Rh = 1/9, indicating an increase in the reducibility of Rh species. Surface chemical analysis by X-ray absorption spectroscopy (XANES and EXAFS) and XPS revealed that Rh species in the Ir-Rh/CeO_2-ZrO_2 samples is mainly present as Rh_2O_3 nanoparticles and that the surface of Rh species is in the catalytically active reducing state by interacting with Ir. Although an appearance of IR bands due to a gem-dicarbonyl species on Rh^+ ($Rh^+(CO)_2$) was predominantly observed when CO was adsorbed on Rh/CeO_2-ZrO_2, strong IR band due to CO species linearly bonded on Rh^0 was observed for Ir-Rh/CeO_2-ZrO_2 samples. On the basis of these results, we concluded that the formation of Ir-Rh nanoparticles composed of finely-divided Ir species on the surface of Rh particles with a size of 1 nm was considered to be responsible for high catalytic activity of Ir-Rh/CeO_2-ZrO_2 for NO-CO-C_3H_6-H_2-O_2 reaction.

We finally examined the effect of Ir-Rh loading on the catalytic performance of Ir-Rh/CeO_2-ZrO_2 with Ir/Rh = 1/9 for the three-way catalytic reactions, and found that Ir-Rh/CeO_2-ZrO_2 showed still high catalytic performance as Ir-Rh loading was decreased to 0.3 wt%. Ir-Rh/CeO_2-ZrO_2 is effective catalyst leading to minimize the Rh usage.

Acknowledgements

This study was supported by a Grant–in–Aid for Scientific Research (No. 24651077) from the Ministry of Education, Culture, Sports, Science and Technology of Japan. The authors thank Ms. Atsuki Kon, Ms. Chizuko Tanaka, Ms. Sachi Ikemoto and Dr. Chizuko Maeda of JFE Techno-Research Corporation for their assistance in XAFS and STEM/HAADF/EDS measurements.

Notes and references

[a] *Advanced Ceramics Research Center, Nagoya Institute of Technology, 10-6-29 Asahigaoka, Tajimi, Gifu 507-0071, Japan.*
[b] *The Institute of Scientific and Industrial Research, Osaka University, 8-1 Mihogaoka, Ibaraki, Osaka 567-0047, Japan.*
[c] *EcoTopia Science Institute, Nagoya University, Furo-cho, Chikusa-ku, Nagoya 464-8603, Japan.*
* *Corresponding author: Tel: +81-572-27-9964, Fax: +81-572-27-6812, E-mail: haneda.masaaki@nitech.ac.jp*
† *Electronic supplementary information (ESI) available.*

1 J.T. Kummer, *Prog. Energy Combust. Sci.*, 1979, **6**, 177.
2 D. Jollie, *PLATINUM 2010*, Johnson Matthey, UK, 2010, p. 44.
3 K.C. Taylor, *Catal. Rev.–Sci. Eng.*, 1993, **35**, 457.
4 M. Shelef and G.W. Graham, *Catal. Rev.–Sci. Eng.*, 1994, **36**, 433.
5 M. Haneda, K. Shinoda, A. Nagane, O. Houshito, H. Takagi, Y. Nakahara, K. Hiroe, T. Fujitani and H. Hamada, *J. Catal.*, 2008, **259**, 223.
6 I. Heo, D.Y. Yoon, B.K. Cho, I.-S. Nam, J.W. Choung and S. Yoo, *Appl. Catal. B*, 2012, **121-122**, 75.
7 H. Kawabata, Y. Koda, H. Sumida, M. Shigetsu, A. Takami and K. Inumaru, *Chem. Commun.*, 2013, **49**, 4015.
8 H. Kawabata, Y. Koda, H. Sumida, M. Shigetsu, A. Takami and K. Inumaru, *Catal. Sci. Technol.*, 2014, **4**, 697.
9 T. Tanabe, A. Morikawa, M. Hatanaka, N. Takahashi, Y. Nagai, A. Sato, O. Kuno, H. Suzuki and H. Shinjoh, *Catal. Today*, 2012, **184**, 219.
10 M. Machida, K. Murakami, S. Hinokuma, K. Uemura, K. Ikeue, M. Matsuda, M. Chai, Y. Nakahara and T. Sato, *Chem. Mater.*, 2009, **21**, 1796.
11 K. Ikeue, K. Murakami, S. Hinokuma, K. Uemura, D.Zhang and M. Machida, *Bull. Chem. Soc. Jpn.*, 2010, **83**, 291.
12 S. Hinokuma, M. Okamoto, E. Ando, K. Ikeue and M. Machida, *Catal. Today*, 2011, **175**, 593.
13 M. Haneda, H. Sawada, N. Kamiuchi and M. Ozawa, *Chem. Lett.*, 2013, **42**, 60.
14 S. Bernal, J.J. Calvino, M.A. Cauqui, J.M. Gatica, C. Larese, J.A. Pérez Omil and J.M. Pintado, *Catal. Today*, 1999, **50**, 175.
15 H. Shinjoh, *Catal. Surv. Asia*, 2009, **13**, 184.
16 L. Cao, C. Ni, Z. Yuan and S. Wang, *Catal. Commun.*, 2009, **10**, 1192.
17 J.-R. Kim, W.-J. Myeong and S.-Ki. Ihm, *J. Catal.*, 2009, **263**, 123.
18 F. Zhong, Y. Xiao, X. Weng, K. Wei, G. Cai, Y. Zheng and Q. Zheng, *Catal. Lett.*, 2009, **133**, 125.
19 K. Tanimoto, H. Kato, S. Takeshita, M. Hidaka, S. Hinokuma and M. Machida, Bull. *Chem. Soc. Jpn.*, 2013, **86**, 1327.
20 A.V. Vedyagin, M.S. Garvilov, A.M. Volodin. V.O. Stoyanovskii, E.M. Slavinskaya, I.V. Mishakov and Y.V. Shubin, *Top. Catal.*, 2013, **56**, 1008.
21 Y. Renème, F. Dhainaut and P. Granger, *Appl. Catal. B*, 2012, **111-112**, 424.
22 P.S. Dimick, J.L. Kross, E.G. Roberts, R.G. Herman, H.G. Stenger and C.E. Lyman, *Appl. Catal. B*, 2009, **89**, 1.
23 J.Y. Park, Y. Zhang, S.H. Joo, Y. Jung and G.A. Somorjai, *Catal. Today*, 2012, **181**, 133.
24 J.R. Renzas, W. Huang, Y. Zhang, M.E. Grass and A.A. Somorjai, *Catal. Lett.*, 2011, **141**, 235.
25 M.D. Amiridis, C. Mihut, M. Maciejewski and A. Baiker, *Top. Catal.*, 2004, **28**, 141.
26 H. Hamada and M. Haneda, *Appl. Catal. A*, 2012, **421-422**, 1.
27 M. Haneda, Pusparatu, Y. Kintaichi, I. Nakamura, M. Sasaki, T. Fujitani and H. Hamada, *J. Catal.*, 2005, **229**, 197.
28 M. Haneda and H. Hamada, *J. Catal.*, 2010, **273**, 39.
29 T. Fujitani, I. Nakamura, Y. Kobayashi, A. Takahashi, M. Haneda and H. Hamada, *J. Phys. Chem. B*, 2005, **109**, 17603.
30 T. Fujitani and I. Nakamura, *Catal. Surv. Asia*, 2009, **13**, 22.
31 W. Chen, Q. Shen, R.A. Bartunski, P. Kaghazchi and T. Jacob, *ChemPhysChem*, 2011, **11**, 2515.
32 M. Haneda, N. Aoki, M. Sasaki, H. Hamada and M. Ozawa, *Appl. Catal. A*, 2011, **394**, 239.
33 N. Kamiuchi, M. Haneda and M. Ozawa, *Catal. Today*, 2013, **201**, 79.
34 M. Yashima, H. Arashi, M. Kakihana and M. Yoshimura, *J. Am. Ceram. Soc.*, 1994, **77**, 1067.
35 R. Si, Y.-W. Zhang, S.-J. Li, B.-X. Liu and C.-H. Yan, *J. Phys. Chem. B*,

2004, **108**, 12481.
36 S. Damyanova, B. Pawlec, K. Arishtirova, M.V. Martinez Huerta and J.L.G. Fierro, *Appl. Catal. A*, 2008, **337**, 86.
37 S.C. Chan, S.C. Fung and J.H. Sinfelt, *J. Catal.*, 1988, **113**, 164.
38 S. Musić, S. Popović, M. Maljković, Ž. Skoko, K. Furić and A. Gajović, *Mater. Lett.*, 2003, **57**, 4509.
39 Y. Liu, F.-Y. Huang, J.-M. Li, W.-Z. Weng, C.-R. Luo, M.-L. Wang, W.-S. Xia, C.-J. Huang and H.-L. Wan, *J. Catal.*, 2008, **256**, 192.
40 D. Martin and D. Duprez, *Appl. Catal. A*, 1995, **131**, 297.
41 M. Ferrandon and T. Krause, *Appl. Catal. A*, 2006, **311**, 135.
42 S. Pitkäaho, L. Matejova, K. Jiratova, S. Ojala and R.L. Keiski, *Appl. Catal. B*, 2012, **126**, 215.
43 K. Dohmae, T. Nonaka and Y. Seno, *Surf. Interface Anal.*, 2005, **37**, 115.
44 G. Lafaye, C. Mihut, C. Especel, P. Marécot and M.D. Amiridis, *Langmuir*, 2004, **20**, 10612.
45 D.I. Kondarides, T. Chafik and E. Verykios, *J. Catal.*, 2000, **191**, 147.
46 K. Hadjiivanov, E. Ivanova, L. Dimitrov and H. Knözinger, *J. Mol. Struc.*, 2003, **661-662**, 459.
47 S. Trautmann and M. Baerns, *J. Catal.*, 1994, **150**, 335.
48 C.A. Rice, S.D. Worley, C.W. Curtis, J.A. Guin and A.R. Tarrer, *J. Phys. Chem.*, 1981, **74**, 6487.
49 G.N. Vayssilov and N. Rösch, *J. Am. Chem. Soc.*, 2002, **124**, 3783.
50 J. Raskó and J. Bontovics, *Catal. Lett.*, 1997, **58**, 27.
51 R.R. Cavanagh and J.T. Yates, Jr., *J. Chem. Phys.*, 1981, **74**, 4150.
52 F. Solymosi and J. Raskó, *J. Catal*., 1980, **62**, 253.
53 F. Solymosi, É. Novák and A. Molnár, *J. Phys. Chem.*, 1990, **94**, 7250.
54 A. Bourane, M. Nawdali and D. Bianchi, *J. Phys. Chem. B*, 2002, **106**, 2665.
55 R.F. van Slooten and B.E. Nieuwenhuys, *J. Catal.*, 1990, **122**, 429.

[Colour Graphic]

Improved three-way catalytic activity of bimetallic Ir-Rh catalyst supported on CeO_2-ZrO_2

Masaaki Haneda*, Takahiro Kaneko, Naoto Kamiuchi, Masakuni Ozawa

The addition of a small amount of Ir caused a significant increase in the TWC performance of Rh/CeO_2-ZrO_2.